Measuring Local Electric Fields and Local Charge Densities at Electrode Surfaces using Graphene-enhanced Raman Spectroscopy (GERS)-based Stark-shifts

Haotian Shi[a], Bofan Zhao[b], Jie Ma[c], Mark J. Bronson Jr.[d], Zhi Cai[c], Jihan Chen[b], Yu Wang[c], Maximum Cronin[b], Lasse Jensen[d] and Stephen B. Cronin*[a,b]

[a]Department of Chemistry, [b]Ming Hsieh Department of Electrical Engineering,
[c]Department of Materials Science, University of Southern California,
Los Angeles, CA 90089
[d]Department of Chemistry, Pennsylvania State University,
University Park, PA 16802
Corresponding Author's Email Address: scronin@usc.edu

Abstract:

We report spectroscopic measurements of the local electric fields and local charge densities at electrode surfaces using graphene-enhanced Raman spectroscopy (GERS) based on the Stark-shifts of surface-bound molecules and the *G* band frequency shift in graphene. Here, monolayer graphene is used as the working electrode in a three-terminal potentiostat while Raman spectra are collected *in situ* under applied electrochemical potentials using a water immersion lens. First, a thin layer (1Å) of copper (II) phthalocyanine (CuPc) molecules are deposited on monolayer graphene by thermal evaporation. GERS spectra are then taken in an aqueous solution as a function of the applied electrochemical potential. The shifts in vibrational frequencies of the graphene *G* band and CuPc are obtained simultaneously and correlated. The upshifts in the *G* band Raman mode are used to determine the free carrier density in the graphene sheet under these applied potentials. Of the three dominant peaks in the Raman spectra of CuPc (i.e., 1531, 1450, and 1340 cm^{-1}), only the 1531 cm^{-1} peak exhibits Stark-shifts and can, thus, be used to report the local electric field strength at the electrode surface under electrochemical

working conditions. Between applied electrochemical potentials from -0.8V to 0.8V vs. NHE, the free carrier density in the graphene electrode spans a range from -4×10^{12} cm^{-2} to 2×10^{12} cm^{-2}. Corresponding Stark-shifts in the CuPc peak around 1531 cm^{-1} are observed up to 1.0 cm^{-1} over a range of electric field strengths between -3.78×10^{6} and 1.85×10^{6} V/cm. Slightly larger Stark-shifts are observed in a 1M KCl solution, compared to those observed in DI water, as expected based on the higher ion concentration of the electrolyte. Based on our data, we determine the Stark shift tuning rate to be 0.178 cm^{-1}/ (10^{6} V/cm), which is relatively small due to the planar nature of the CuPc molecule, which largely lies perpendicular to the electric field at this electrode surface. Computational simulations using density functional theory (DFT) predict similar Stark shifts and provide a detailed atomistic picture of the electric field-induced perturbations to the surface-bound CuPc molecules.

Keywords: GERS, Stark-shifts, local electric field, *in-situ* Raman, monolayer graphene

Introduction:

Raman spectroscopy is an important tool for measuring the vibrational signatures of molecules for chemical detection and for characterizing nanoscale materials like graphene, transition metal dichalcogenides, and carbon nanotubes.[1-6] The discovery of surface-enhanced Raman scattering (SERS) in the 1970s[7-11] was, in fact, an early manifestation of nanoscale enhancement with reports of increases in the Raman signal by as much as 10^{14} and robust demonstrations of single-molecule detection.[12-17] In SERS, there are two mechanisms of enhancement that are generally accepted: 1) an electromagnetic mechanism (EM), which originates from the local electromagnetic field enhancement on rough metal surfaces and metal nanoparticles, and 2) a chemical enhancement mechanism (CE), which arises from the dynamic transfer of charge through interaction between the target molecule and underlying metal.[18-21] The EM enhancement typically arises when the incident light matches a plasmon resonance within the metal nanostructure, which can produce fields as much as 1000 times higher than the incident electromagnetic fields for Au and Ag nanoparticles.[22-24] While the EM enhancement produces an overall uniform enhancement of all the Raman modes, the chemical enhancement depends on the symmetry of each vibrational mode, and therefore produces a vibrational-mode-specific enhancement, which makes SERS spectra appear quite different from bulk solution Raman spectra.

In 2010, monolayer graphene was shown to enhance the Raman signal of adsorbed molecules by as much as 2 orders of magnitude, including phthalocyanine (Pc), rhodamine 6G (R6G), protoporphyin IX (PPP), and crystal violet (CV).[25, 26] Since graphene is largely optically inert with only 2.3% absorption in the visible range and plasmon resonances that lie in the infrared wavelength range,[27, 28] it is believed that EM enhancement is minimal in this material

system.[25, 26] For GERS, this distinction is further supported by the fact that molecules with large GERS enhancement factors can be correlated with their symmetry groups.[29] The Raman signals of molecules on multilayer graphene show no enhancement and are even weaker than those molecules on a Si/SiO_2 substrate.[29,30,31] It should be noted that the underlying chemical enhancement mechanism associated with this GERS phenomenon is still not fully understood.

In our previous work, we measured Raman spectra at a graphene/water interface as a function of electrochemical potential.[32] Large electrostatic fields exist at the surface of these electrodes due to the double layer at this solid/liquid interface.[33] Various chemical reactions entail the transfer of charged or polarized reactants across this interface. Electric fields can, therefore, have a significant effect on these reaction mechanisms and catalysis, which are intimately related to the local electric field strength. In a previous study by Dawlaty et al., sum frequency generation (SFG) spectroscopy was used to explore the interfacial solvation effects on the C-N frequency shift of 4-mercaptobenzonitrile (4-MBN) bound to gold electrode surfaces.[33, 34] Lian and coworkers also used *in situ* SFG probes to characterize the electric fields at solid/liquid interfaces.[35] In a more recent study, Shi et al. demonstrated the local electric fields generated at graphene electrode surfaces can be obtained using surface enhanced Raman scattering, which is a far more facile technique than SFG spectroscopy.[36]

In the work reported here, we explore the effect of applied electrochemical potential and the associated electric fields on a GERS system using CuPc molecules. This approach takes advantage of the unique ability of monolayer graphene to host adsorbed molecules of copper phthalocyanine (CuPc) and provide amplification/enhancement of its Raman signal via the GERS phenomena. The monolayer graphene also serves as a highly-conductive electrode material, enabling us to externally apply an electrochemical potential, while monitoring CuPc's

vibrational modes *in situ*. Despite the sparse coverage of the surface adsorbed molecules, the Raman spectra of the CuPc molecules can easily be observed using a water immersion lens. In addition, the *G* band Raman shift of the graphene is used to report the charge density on the electrode, which is proportional to the local electric field strength. This general approach can be applied to a wide range of molecules that can be used to report various aspects of charge transfer, local pH, and ion concentration.

Experimental Details:

Monolayer graphene was grown by chemical vapor deposition (CVD) at 1000°C in methane and H_2 gas on copper foil at a reduced pressure of 1-1.5 Torr.[37] The copper foil with graphene was then coated with a thin protection layer of PMMA-A6 by spin-coating at 2000 rpm for 45s and then baking at 150°C for 5 minutes. Copper etchant was used to etch away the copper from the bottom of the "sandwich" structure, resulting in a graphene/PMMA film that is left floating on the surface of the liquid copper etchant. This is then cleaned with 10% hydrochloric acid in DI water.[38] Prior to transferring the graphene, two gold electrodes are deposited on an oxidized silicon substrate (300nm SiO_2) by electron-beam evaporation using a shadow mask to serve as the target substrate. The PMMA-graphene layer was then scooped up on the target substrate connecting both gold electrodes. The sample was then baked at 120°C for 5 minutes to improve adhesion. After this, the PMMA layer was removed by soaking in acetone for 5 minutes. Copper (II) phthalocyanine (CuPc) molecules are then deposited on the graphene by thermal evaporation of a 1Å nominal thickness, which provides sub-monolayer coverage. Copper wires are attached to both gold electrodes enabling this graphene layer to serve as a working electrode in a three-terminal potentiostat setup. In order to monitor any potential electrochemical

degradation of this electrode, we also measure the in-plane resistance of the graphene, which usually lies in the range between 1000 and 3000Ω. The gold contacts are then covered with epoxy so that they are not in direct contact with the electrolyte. The active area of the graphene was about 0.25cm^2 after protection with the epoxy, as illustrated in Figure 1b.

Raman spectra of the graphene electrode were taken with 633nm and 532nm wavelength excitation under applied electrochemical potentials in pure DI water using a water immersion lens, as illustrated in Figure 1a. In order to protect the lens from the solution, it was covered with a 13μm thick Teflon sheet (American Durafilm, Inc.). A three terminal potentiostat (Gamry, Inc.) was used to apply a potential to the graphene working electrode with respect to the reference electrode, as illustrated in Figure 1a. A silver/silver chloride reference electrode and glassy carbon electrode (SPI, Inc.) were used as the reference and counter electrodes, respectively. As a comparison, we also performed the same measurements in a 1M KCl as solution. GERS spectra were collected as a function of the applied electrochemical potential. Since the CuPc molecules are not water soluble, they remain stably bound to the graphene surface in solution during these *in situ* measurements. The Raman spectra of the CuPc were collected with a 633nm wavelength laser, which is resonant with this molecule's absorption. The Raman spectra of the underlying graphene electrode (i.e., *G* band) were collected with a 532nm wavelength laser, without being obscured by the CuPc peaks. The shifts in the *G* band Raman frequency are then used to provide a measure of the electrochemical doping in the graphene monolayer, as described in the Results and Discussion section.

Computational Methods:

We performed computational simulations of the Stark shift tuning rate using the Amsterdam Density Functional (ADF) program package.[39-41] The geometry optimizations and frequency

calculations were carried out using the Becke–Perdew[42, 43] (BP86) exchange-correlation functional with dispersion correction (DFT-D3-BJ) by Grimme[44] and triple-ζ polarized (TZP) Slater-type basis. A hydrogen-terminated graphene sheet was optimized with a large frozen core, and the sheet was forced to be planer by specifying C_s symmetry. In vacuum, the CuPc was optimized with a large frozen core. The optimized CuPc was then placed on the graphene sheet and was allowed to relax while holding the graphene sheet fixed in electric fields in both plus and minus z-directions of various field strengths (-0.001au, -0.0005au, 0au, 0.0005au, 0.001au, in which 1 au=5.14×10^9 V/cm). For each of the optimized geometries, the frequencies of the CuPc vibrational modes were calculated using the Mobile Block Hessian[45, 46] where the graphene sheet had its internal degrees of freedom removed.

Results and Discussion:

The *G* band shift of the underlying graphene is plotted in Figure 2a as a function of reference potential (the left y-axis in Figure 2a). Here, the free carrier concentration is obtained from the *G* band Raman shift using following relations put forth by Das Sarma and Berciaud: $n_e = [(21\Delta\omega_G+75)/11.65]^2\bullet10^{10}$ cm^{-2} and $n_h= [(-18\Delta\omega_G-83)/11.65]^2\bullet10^{10}$ cm^{-2}, where n_e and n_h are the two-dimensional charge densities of electrons and holes, respectively, and $\Delta\omega_G$ is the change in the *G* band Raman frequency with respect to the charge neutrality point with units of cm^{-1}.[47, 48] This 2D charge density on the graphene sheet (in electrons or holes per cm^2) is plotted as a function of the applied voltage on the right axis of Figure 2a.[32, 49] Here, we have indicate the regions over which there are electrons and holes in the graphene. Under the applied electrochemical potentials (-0.8V to 0.8V vs. NHE), the free carrier density in the graphene

electrode, obtained from the shifts in the *G* band frequency, spans a range from -4×10^{12} cm^{-2} to 2×10^{12} cm^{-2}.

Figure 2b shows the vibrational Stark shift of the 1531 cm^{-1} vibrational mode of CuPc plotted as a function of the reference potential, which increases monotonically with increasing potential. The righthand axis plots the local electric field calculated from the free carrier concentration in the graphene, obtained from the graphene *G* band Raman shift (the right y-axis in Figure 2a). We calculate the local electric field at the electrode surface using the formula $\varepsilon=e\sigma/2\epsilon_0\epsilon_r$ for an infinitely charged plane, where ε is electric field strength, *e* is the charge of one electron, ϵ_r is the relative dielectric constant, and ϵ_0 is the permittivity of free space. We also assume that the electric field is zero for the sample in air in order to establish the righthand y-axis in Figure 2b, which spans a range from -3.78×10^6 to 1.85×10^6 V/cm. Here, the CuPc Raman mode around 1531 cm^{-1} exhibits Stark shifts up to 1.0 cm^{-1}. From the data in Figures 2a and 2b, we can relate the Stark shift of the CuPc 1531 cm^{-1} peak to the electric field, as plotted in Figure 2c, which exhibits a Stark tuning rate of 0.178 cm^{-1}/ (10^6 V/cm). It is interesting to note that there is an inflection point near zero electric field in the CuPc Stark shift vs. voltage plot taken in DI water (Figure 2c). This is likely related to the differing abilities of the cations (H^+) and anions (OH^-) to produce a local electric field in the water environment. However, to the 1st order approximation, we treat this as a simple linear relation, which is consistent with our simulation results.

Interestingly, the 1531 cm^{-1} peak is the only Raman mode that exhibits a Stark shift. Figure S1 of the Supporting Information document shows the Raman shift of three different CuPc peaks (1531 cm^{-1}, 1450 cm^{-1} and 1340cm^{-1}) plotted as a function of the applied electrochemical potential. From this data, it is clear that only the 1531 cm^{-1} vibrational mode shows a Stark shift.

According to Basova, et al., these three modes are assigned to different bonds with $\boldsymbol{B}_{1g}$ symmetry: the 1531 cm^{-1} peak corresponds to the C_α-N_β band, 1450 cm^{-1} is from C_β-C_β, C_β-C_γ-H, and 1340cm^{-1} is from C_β-C_β, C_α-C_β-C_β, C_γ-C_δ and C_β-C_γ.[50, 51] These bonds are labeled in detail in Figure S2 of the Supporting Information document. Unlike 1450 cm^{-1} and 1340cm^{-1}, which correspond to bonds inside the macrocycle, the contribution to the 1531 cm^{-1} vibration is mainly given by the displacements of the C_α-N_β-C'_α bridge bonds between the macrocycles.[41] It is possible that the bottom macrocycle vibrational modes lie in the plane of the graphene electrode, which is perpendicular to the electric field direction. However, one of the macrocycles might rotate along one half of the bridge bond C_α-N_β (C'_α-N_β) pulling the other half of the bridge bond N_β-C'_α (N_β-C_α) slightly out of the macrocycle plane, which can thereby feel the effects of the applied electric fields. In our understanding, when electrochemical potential is applied to the graphene-CuPc electrode, either cations (H^+) or anions (OH^-) are accumulated on the surface. They will either attract or repulse the electron-rich isoindole rings in CuPc. If the CuPc planar structure is not perfectly in parallel with the graphene surface, adjacent isoindole rings will have different interaction with the accumulated ions, which leads to the displacement and rotation of the bridge bond. Steric effects may also be the reasons of the rotation of the bridge bonds.

Figure 3 shows the corresponding results of the CuPc-on-graphene electrode obtained in a 1M KCl solution. From Figure 3a, we can also see upshifts (up to 12 cm^{-1}) in the *G* band frequency under negative applied potentials, which is approximately 50% larger the upshifts observed in DI water (8 cm^{-1}). Here, the carrier concentration on the sample surface reaches -8×10^{12} cm^{-2} under -0.8V vs. NHE, which is almost two times as large as that obtained in DI water. However, under positive applied potentials, *G* band upshift is comparable to that of the DI water and the carrier concentration is even smaller. By correlating the CuPc Raman data to the

electric field derived from the graphene *G* band Raman data, we find that both the Stark shift and electric field increase monotonically as a function of the reference potential in a 1M KCl solution, as plotted in Figure 3b. The CuPc peak exhibits Stark shifts up to 1.56 cm^{-1}, over a range of electric field strengths from -7.5×10^6 to 1.2×10^6 V/cm. Figures 3c shows the direct relation between the Stark shift of the CuPc 1531 cm^{-1} peak and the electric field in a 1M KCl solution, which exhibits a Stark tuning rate of 0.184 cm^{-1}/ (10^6 V/cm) . Figure 3d shows a comparison of the Stark shift difference of the 1531cm^{-1} peak of CuP_C plotted as a function reference potential in DI water and 1M KCl solution with their fitted line, the slopes of which give the Stark tuning rate (STR) in units of cm^{-1}/ (10^6 V/cm). The difference between the Stark tuning rates in these different electrolytes is less than 3%, which verifies the validity of this approach. Thus, the local electric field can be directly related to Stark-shift of the 1531cm^{-1} CuPc Raman peaks.

From the computational simulation results, we observe that, for an electric field applied perpendicularly out of the surface, the outer phenyl rings moved away from the surface while the inner carbon-nitrogen ring moved closer to the surface. For an electric field applied perpendicularly into the surface, the outer phenyl rings moved closer to the surface while the inner carbon-nitrogen ring moved away from the surface. In the simulated Raman spectra of CuPc in vacuum, there were five Raman active modes near the 3 peaks seen in the experimental spectra. The calculated Raman spectrum is plotted in Figure 4a, exhibiting peaks at 1546cm^{-1}, 1520cm^{-1}, 1428cm^{-1}, 1418cm^{-1} and 1335cm^{-1}. Atomic scale diagrams of the vibrational modes under applied electric field are shown in Figures S4a-e of the SI, respectively. The 1418cm^{-1} and 1428cm^{-1} modes are the symmetric and asymmetric version of phenyl ring vibration, while the 1520cm^{-1} and 1546cm^{-1} are the symmetric and asymmetric version of carbon-nitrogen stretching.

Of these modes, only the 1546cm^{-1} mode exhibits an appreciable Stark shift. The Stark shift of this mode is plotted as a function of the applied electric field in Figure 4c and exhibits a Stark tuning rate of 0.141cm^{-1}/ (10^6 V/cm). The same can be done for the other modes, as shown in Figures S5b-e of the SI. The other 4 modes result in Stark tuning rates of 0.027 cm^{-1}/(10^6 V/cm), 0.016cm^{-1}/(10^6 V/cm), 0.006cm^{-1}/(10^6 V/cm), and 0.020cm^{-1}/(10^6 V/cm) for the 1520cm^{-1}, 1428cm^{-1}, 1418cm^{-1}, and 1335cm^{-1} modes, respectively, which are at least one order of magnitude smaller than that of 1546cm^{-1} mode. Full experimental and calculated Raman spectra are plotted against each other in Figure S6 of the Supporting Information document. The simulation results of the Stark shifts calculated for the 1546cm^{-1} mode are consistent with our experimental measurements of the 1531cm^{-1} mode. Here, it is important to note that the simulated spectra correspond to the gas phase Raman spectra of CuPc, Therefore, a direct comparison with the experimental GERS spectra is not valid, since the Raman scattering selection rules are changed when the molecules are bound to a surface. In addition, we only used the gas phase spectra to identify the normal modes of the graphene-CuPc complex that were likely to be Raman active and give support that the 1546cm^{-1} mode corresponded to the mode that we found in experiment. In our experiment, only the 1531cm^{-1} mode shows an apparent Stark shift-electric field dependence, and more importantly, the STR 0.141 is reasonably close to the experimental data 0.178, which verifies the applicability of this approach. The raw Raman spectra taken under 633nm and 532nm excitations are shown in Figures S7 and S8 in the SI document, clearly showing the Stark shift of CuPc and the Raman shift of graphene G band.

We would like to point out that our previous work using graphene alone to monitor local electric fields via the relation $E=\sigma/2\varepsilon$, relied on the assumption that ε is known, which is true to bulk water but not necessarily at the electrode surface.[32] It is, therefore, important to develop

other probes to report the local electric field at electrode surfaces. Here, we chose CuPc for this study because it is a strongly GERS-enhanced molecule.[25] However, its planar structure results in relatively small Stark tuning rates. One of the key insights provided by the DFT calculations is a slight bond rotation out of plane that makes this particular Raman mode Stark sensitive.

Conclusion:

In summary, we report spectroscopic measurements of the local electric fields and local charge densities at electrode surfaces using graphene-enhanced Raman spectroscopy (GERS) based on the Stark-shifts of surface-bond molecules and the *G* band frequency in monolayer graphene. GERS spectra are then taken in an aqueous solution systematically as a function of the applied electrochemical potential. The information from the shifts in both the graphene *G* band and CuPc vibrational frequencies are obtained simultaneously and correlated. The carrier density in the graphene sheet is used to determine the upshifts in the *G* band Raman mode under these applied potentials. Of the three dominant peaks in the Raman spectra of CuPc (at 1531, 1450, and 1340cm^{-1}), only the 1531 cm^{-1} peak exhibits Stark-shifts and is used to report the local electric field strength at the electrode surface under electrochemical working conditions. Under the applied electrochemical potentials between -0.8V to 0.8V vs. NHE, the free carrier density in the graphene electrode is obtained from the shifts in the *G* band frequency and spans a range from -4×10^{12} cm^{-2} to 2×10^{12} cm^{-2}. Corresponding Stark-shifts in the CuPc peak (around 1531 cm^{-1}) are observed up to 1.0 cm^{-1}over a range of electric field strengths between -3.78×10^{6} to 1.85×10^{6} V/cm. About 56% larger Stark-shifts and 54% larger local electric fields are observed in a 1M KCl solution, compared to those observed in DI water, as expected based on the higher ion

concentration of the electrolyte. Despite these larger shifts and larger electric fields, the Stark tuning rates observed in DI water and 1M KCl solutions agree within 3% of each other, which verifies the validity of this approach. Density functional theory calculations predict 5 Raman active modes for CuPc-on-graphene, only one of which exhibits a Stark shift. The vibrational frequency and Stark tuning rate of this mode agrees well with the experimental values.

Supporting Information:

Raman shift of different CuPc peaks plotted as a function of the applied electrochemical voltage, measured in water and in 1mol/L KCl solution; Cartesian coordinate axes orientation and bond lengths (in Å) (replotted from Figure 1a of the work by Basova et al[50, 51]; Capacitance-voltage plot of the CuPc graphene-based electrode measured in DI water; Carrier density obtained from the capacitance-voltage data (i.e., Q=CV) plotted together with the carrier density obtained by Raman spectroscopy; Atomic diagrams of the five Raman active vibrational modes calculated for CuPc at 1546cm^{-1}, 1520cm^{-1}, 1428cm^{-1}, 1418cm^{-1}, 1335cm^{-1} vibrational modes; CuPc peaks different vibrational modes at 1546cm^{-1}, 1520cm^{-1}, 1428cm^{-1}, 1418cm^{-1}, 1335cm^{-1} plotted as a function of electric field with their calculated Stark tuning rates (STRs); Experimental and Simulated CuPc Raman spectra in DI water; All three main modes and zoomed-in version of 1531cm^{-1} mode; Water fall plot of Stark-shift Raman spectra (633nm) of CuPc are shown in DI water; All three main modes and zoomed-in version of G band mode of graphene Raman spectra (532nm) in DI water.

Acknowledgements:

This research was supported by the National Science Foundation (NSF) award no. 1708581 (H.S.) and CBET-1512505 (J.C.), Air Force Office of Scientific Research (AFOSR) grant no. FA9550-15-1-0184 (B.Z.), Army Research Office (ARO) award no. W911NF-17-1-0325 (Z.C.), U.S. Department of Energy, Office of Science, Office of Basic Energy Sciences, and award no. DE-SC0019322 (Y.W.). We would like to thank Prof. Mark Thompson for a valuable discussion and use of deposition facilities. L.J. and M.B. acknowledge the support from the National Science Foundation Grant CHE-1707657 and NRT-1449785. Portions of this work were conducted with Advanced Cyberinfrastructure computational resources provided by The Institute for Cyber-Science at The Pennsylvania State University (https://ics.psu.edu/).

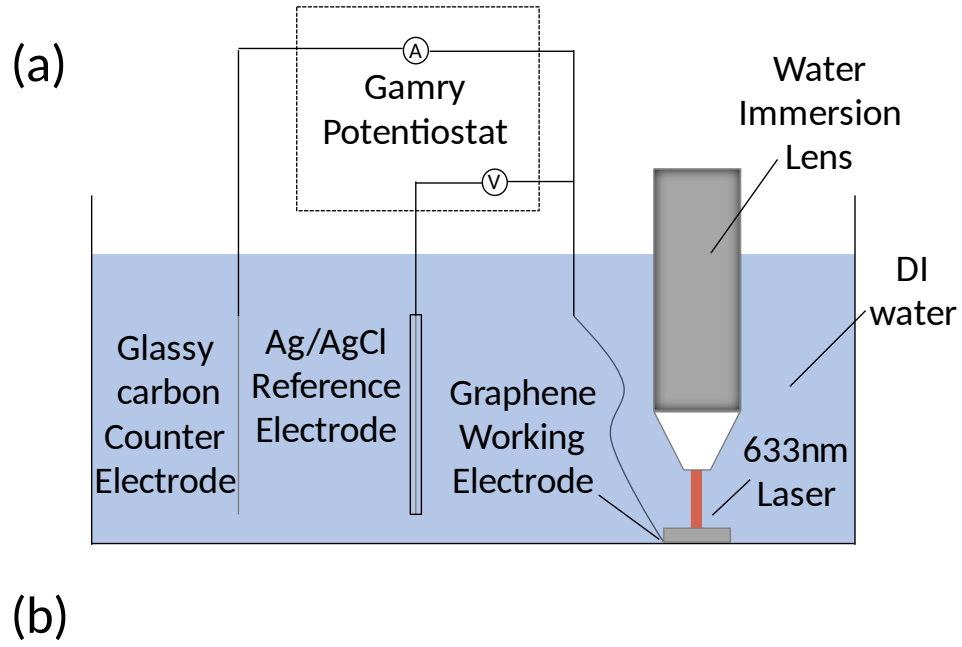

Figure 1. Schematic diagrams of the (a) three-terminal photoelectrochemical cell using a water immersion lens to obtain Raman Spectra *in situ* and (b) CuPc-coupled monolayer graphene electrode.

(a)

(b)

(c)

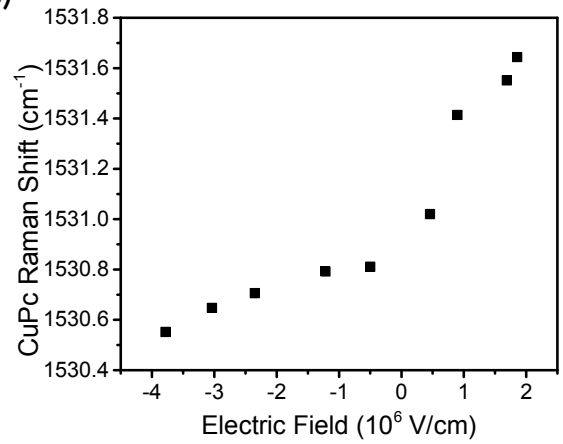

Figure 2. (a) Graphene *G* band Raman shift (black) and the free carrier concentration (red) plotted as a function of the applied potential. (b) CuPc Stark-shift (black) and the electric field (red) plotted as a function of the applied potential measured in DI water. (c) CuPc 1531cm^{-1} peak plotted as a function of electric field at the monolayer graphene electrode surface.

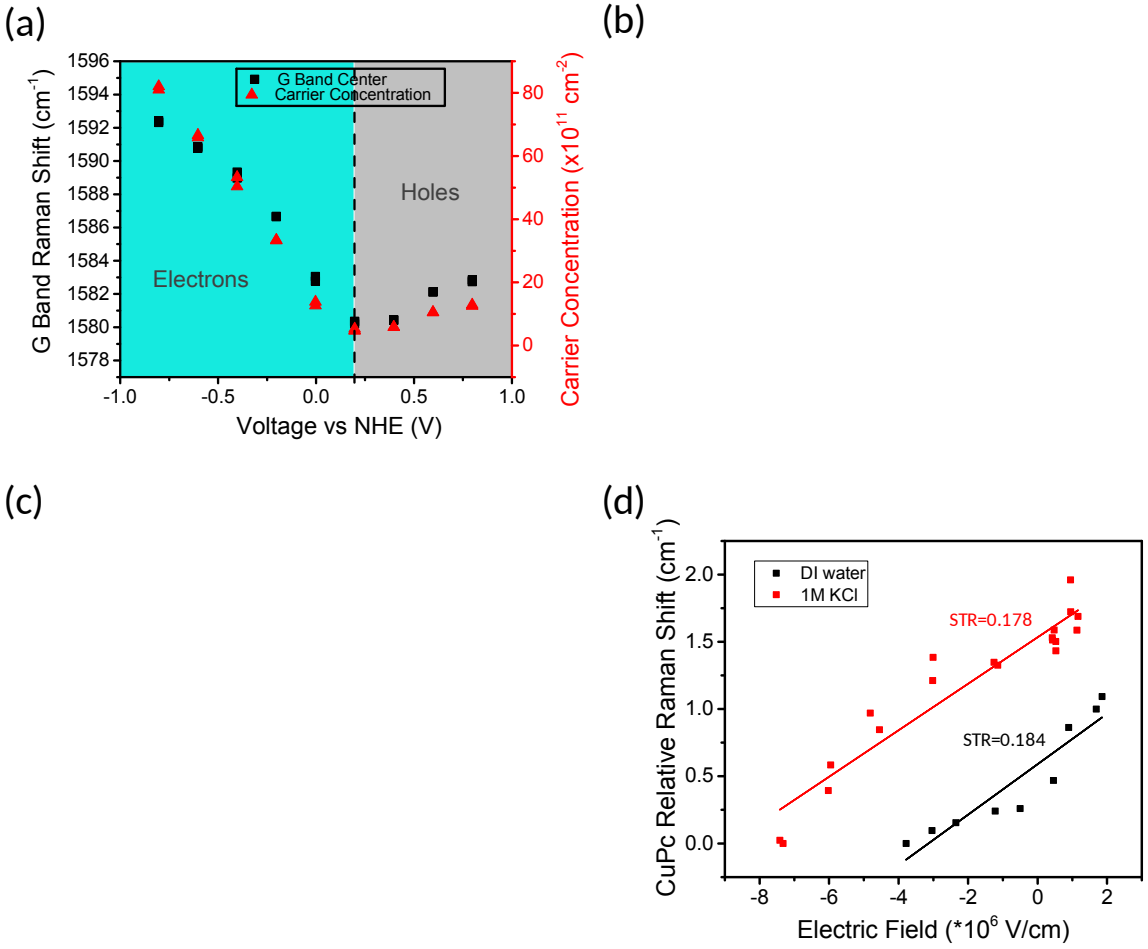

Figure 3. (a) Graphene *G* band Raman shift (black) and the free carrier concentration (red) plotted as a function of the applied potential measured in 1M KCl solution. (b) CuPc Stark-shift (black) and the electric field (red) plotted as a function of the applied potential measured in 1M KCl solution. (c) CuPc 1531cm^{-1} peak plotted as a function of electric field at the graphene

electrode surface. (d) CuPc Stark-shift change plotted as a function of the applied voltage, measured in DI water (black) and in KCl (red) plotted together with their linear fits, which give the Stark tuning rates (STRs) in units of $cm^{-1}/(10^6$ V/cm).

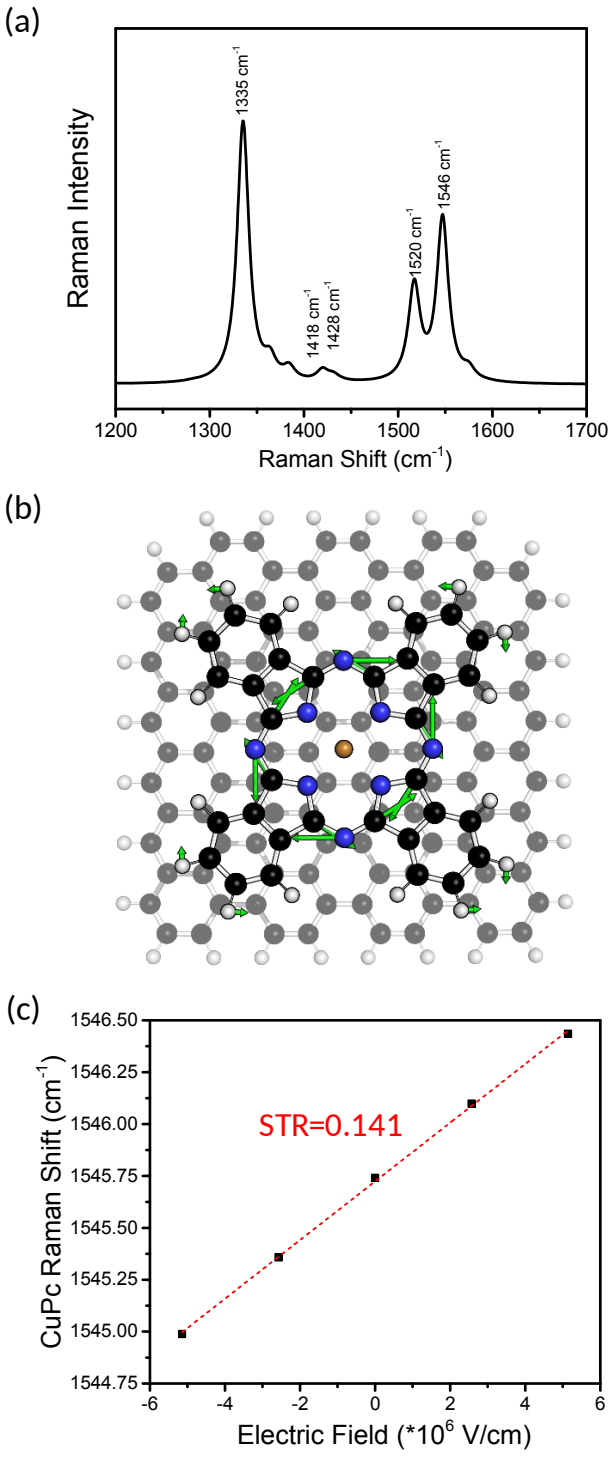

Figure 4. ADF-calculated (a) CuPc Raman spectra, (b) CuPc Raman Shift 1546cm^{-1} vibrational mode versus the applied electric field, (c) CuPc 1546cm^{-1} peak plotted as a function of electric field with the Stark tuning rate at the graphene electrode surface.

References

1. Malard, L. M.; Pimenta, M. A.; Dresselhaus, G.; Dresselhaus, M. S., Raman Spectroscopy in Graphene. *Phys. Rep.* **2009**, 473, 51-87.
2. Dresselhaus, M. S.; Jorio, A.; Hofmann, M.; Dresselhaus, G.; Saito, R., Perspectives on Carbon Nanotubes and Graphene Raman Spectroscopy. *Nano Lett.* **2010**, 10, 751-758.
3. Dresselhaus, M. S.; Jorio, A.; Saito, R., Characterizing Graphene, Graphite, and Carbon Nanotubes by Raman Spectroscopy. *Annu. Rev. Condens.* **2010**, 1, 89-108.
4. Dhall, R.; Neupane, M. R.; Wickramaratne, D.; Mecklenburg, M.; Li, Z.; Moore, C.; Lake, R. K.; Cronin, S., Direct Bandgap Transition in Many-Layer MoS_2 by Plasma-Induced Layer Decoupling. *Adv. Mater.* **2015**, 27, 1573-1578.
5. Dhall, R.; Li, Z.; Kosmowska, E.; Cronin, S. B., Charge Neutral Mos_2 Field Effect Transistors Through Oxygen Plasma Treatment. *J. Appl. Phys* **2016**, 120, 195702.
6. Dhall, R.; Seyler, K.; Li, Z.; Wickramaratne, D.; Neupane, M. R.; Chatzakis, I.; Kosmowska, E.; Lake, R. K.; Xu, X.; Cronin, S. B., Strong Circularly Polarized Photoluminescence from Multilayer MoS_2 Through Plasma Driven Direct-Gap Transition. *ACS Photonics* **2016**, 3, 310-314.
7. Campion, A.; Kambhampati, P., Surface-Enhanced Raman Scattering. *Chem. Soc. Rev.* **1998**, 27, 241-250.
8. Moskovits, M., Surface-Enhanced Raman Spectroscopy: A Brief Retrospective. *J. Raman Spectrosc.* **2005**, 36, 485-496.
9. Otto, A.; Mrozek, I.; Grabhorn, H.; Akemann, W., Surface-Enhanced Raman Scattering. *J. Condens.* **1992**, 4, 1143.
10. Efremov, E. V.; Ariese, F.; Gooijer, C., Achievements in Resonance Raman Spectroscopy: Review of a Technique with a Distinct Analytical Chemistry Potential. *Anal. Chim. Acta* **2008**, 606, 119-134.
11. Petry, R.; Schmitt, M.; Popp, J., Raman Spectroscopy—A Prospective Tool in the Life Sciences. *ChemPhysChem* **2003**, 4, 14-30.
12. Nie, S.; Emory, S. R., Probing Single Molecules and Single Nanoparticles by Surface-Enhanced Raman Scattering. *Science* **1997**, 275, 1102.
13. Kneipp, K.; Wang, Y.; Kneipp, H.; Perelman, L. T.; Itzkan, I.; Dasari, R.; Feld, M. S., Single Molecule Detection using Surface-Enhanced Raman Scattering (SERS). *Phys. Rev. Lett.* **1997**, 78, 1667-1670.
14. Dieringer, J. A.; Lettan, R. B.; Scheidt, K. A.; Van Duyne, R. P., A Frequency Domain Existence Proof of Single-Molecule Surface-Enhanced Raman Spectroscopy. *J. Am. Chem. Soc.* **2007***, 129, 16249-16256.*
15. Jiang; Bosnick, K.; Maillard, M.; Brus, L., Single Molecule Raman Spectroscopy at the Junctions of Large Ag Nanocrystals. *J. Phys. Chem. B* **2003**, 107, 9964-9972.
16. Xu, H.; J. Bjerneld, E.; Käll, M.; Börjesson, L., Spectroscopy of Single Hemoglobin Molecules by Surface Enhanced Raman Scattering. *Phys. Rev. Lett.* **1999**, 83, 4357-4360.
17. Michaels, A. M.; Jiang; Brus, L., Ag Nanocrystal Junctions as the Site for Surface-Enhanced Raman Scattering of Single Rhodamine 6G Molecules. *J. Phys. Chem. B* **2000**, 104, 11965-11971.
18. Persson, B. N. J.; Zhao, K.; Zhang, Z., Persson, Zhao, and Zhang Reply. *Phys. Rev. Lett.* **2006**, 97, 199702.

19. Le Ru, E. C.; Etchegoin, P. G., Comment on Chemical Contribution to Surface-Enhanced Raman Scattering. *Phys. Rev. Lett.* **2006**, 97, 199701.
20. Wu, D. Y.; Liu, X. M.; Duan, S.; Xu, X.; Ren, B.; Lin, S. H.; Tian, Z. Q., Chemical Enhancement Effects in SERS Spectra: A Quantum Chemical Study of Pyridine Interacting with Copper, Silver, Gold and Platinum Metals. *J. Phys. Chem. C* **2008**, 112, 4195-4204.
21. Sun, M.; Liu, S.; Chen, M.; Xu, H., Direct Visual Evidence for the Chemical Mechanism of Surface-Enhanced Resonance Raman Scattering via Charge Transfer. *J. Raman Spectrosc.* **2009**, 40, 137-143.
22. Pavaskar, P.; Theiss, J.; Cronin, S. B., Plasmonic Hot Spots: Nanogap Enhancement vs. Focusing Effects from Surrounding Nanoparticles. *Opt. Express* **2012**, 20, 14656-14662.
23. Pavaskar, P.; Hsu, I. K.; Theiss, J.; Hung, W. H.; Cronin, S. B., A Microscopic Study Of Strongly Plasmonic Au And Ag Island Thin Films. *J. Appl. Phys.* **2013**, 113, 034302.
24. Liu, Z.; Hou, W.; Pavaskar, P.; Aykol, M.; Cronin, S., Plasmon Resonant Enhancement of Photocatalytic Water Splitting Under Visible Illumination. *Nano Lett.* **2011**, 11, 1111.
25. Ling, X.; Xie, L. M.; Fang, Y.; Xu, H.; Zhang, H. L.; Kong, J.; Dresselhaus, M. S.; Zhang, J.; Liu, Z. F., Can Graphene Be Used as a Substrate for Raman Enhancement? *Nano Lett.* **2010**, 10, 553-561.
26. Huang, S. X.; Ling, X.; Liang, L. B.; Song, Y.; Fang, W. J.; Zhang, J.; Kong, J.; Meunier, V.; Dresselhaus, M. S., Molecular Selectivity of Graphene-Enhanced Raman Scattering. *Nano Lett.* **2015**, 15, 2892-2901.
27. Brar, V. W.; Jang, M. S.; Sherrott, M.; Lopez, J. J.; Atwater, H. A., Highly Confined Tunable Mid-Infrared Plasmonics in Graphene Nanoresonators. *Nano Lett.* **2013**, 13, 2541-2547.
28. Yan, H.; Li, X.; Chandra, B.; Tulevski, G.; Wu, Y.; Freitag, M.; Zhu, W.; Avouris, P.; Xia, F., Tunable Infrared Plasmonic Devices using Graphene/Insulator Stacks. *Nat. Nanotechnol.* **2012**, 7, 330.
29. Ling, X.; Xie, L.; Fang, Y.; Xu, H.; Zhang, H.; Kong, J.; Dresselhaus, M. S.; Zhang, J.; Liu, Z., Can Graphene be used as a Substrate for Raman Enhancement? *Nano Lett.* **2010**, 10, 553-561.
30. Kröger, I.; Stadtmüller, B.; Stadler, C.; Ziroff, J.; Kochler, M.; Stahl, A.; Pollinger, F.; Lee, T.-L.; Zegenhagen, J.; Reinert, F.; Kumpf, C., Submonolayer Growth of Copper-Phthalocyanine on Ag(111). *New J. Phys.* **2010**, 12, 083038.
31. Xu, H.; Xie, L.; Zhang, H.; Zhang, J., Effect of Graphene Fermi Level on the Raman Scattering Intensity of Molecules on Graphene. *ACS Nano.* **2011**, 5, 5338-5344.
32. Shi, H.; Poudel, N.; Hou, B.; Shen, L.; Chen, J.; Benderskii, A. V.; Cronin, S. B., Sensing Local pH and Ion Concentration at Graphene Electrode Surfaces using In-Situ Raman Spectroscopy. *Nanoscale.* **2018**, 10, 2398-2403.
33. Sorenson, S. A.; Patrow, J. G.; Dawlaty, J. M., Solvation Reaction Field at the Interface Measured by Vibrational Sum Frequency Generation Spectroscopy. *J. Am. Chem. Soc.* **2017**, 139, 2369-2378.
34. Patrow, J. G.; Sorenson, S. A.; Dawlaty, J. M., Direct Spectroscopic Measurement of Interfacial Electric Fields near an Electrode under Polarizing or Current-Carrying Conditions. *J. Phys. Chem. C* **2017**, 121, 11585-11592.
35. Ge, A.; Videla, P. E.; Lee, G. L.; Rudshteyn, B.; Song, J.; Kubiak, C. P.; Batista, V. S.; Lian, T., Interfacial Structure and Electric Field Probed by in Situ Electrochemical Vibrational Stark Effect Spectroscopy and Computational Modeling. *J. Phys. Chem. C* **2017**, 121, 18674-18682.

36. Shi, H.; Cai, Z.; Patrow, J.; Zhao, B.; Wang, Y.; Wang, Y.; Benderskii, A.; Dawlaty, J.; Cronin, S. B., Monitoring Local Electric Fields at Electrode Surfaces Using Surface Enhanced Raman Scattering-Based Stark-Shift Spectroscopy during Hydrogen Evolution Reactions. *ACS Appl. Mater. Interfaces* **2018**, 10, 33678-33683.
37. Soo Min, K.; Allen, H.; Yi-Hsien, L.; Mildred, D.; Tomás, P.; Ki Kang, K.; Jing, K., The Effect Of Copper Pre-Cleaning On Graphene Synthesis. *Nanotechnology* **2013**, 24, 365602.
38. Chen, C.-C.; Chang, C.-C.; Li, Z.; Levi, A. F. J.; Cronin, S. B., Gate Tunable Graphene-Silicon Ohmic/Schottky Contacts. *Appl. Phys. Lett.* **2012**, 101, 223113.
39. Te Velde, G.; Bickelhaupt, F. M.; Baerends, E. J.; Fonseca Guerra, C.; van Gisbergen, S. J. A.; Snijders, J. G.; Ziegler, T., Chemistry with ADF. *J. Comput. Chem.* **2001**, 22, 931-967.
40. Fonseca Guerra, C.; Snijders, J. G.; te Velde, G.; Baerends, E. J., Towards an Order-N DFT Method. *Theor. Chem. Acc* **1998**, 99, 391-403.
41. E.J. Baerends, et al. *ADF* **2019**, Theoretical Chemistry, Vrije Universiteit, Amsterdam, The Netherlands.
42. Becke, A. D., Density-Functional Exchange-Energy Approximation with Correct Asymptotic Behavior. *Phys. Rev. A* **1988**, 38, 3098-3100.
43. Perdew, J. P., Density-Functional Approximation for the Correlation Energy of The Inhomogeneous Electron Gas. *Phys. Rev. B* **1986**, 33, 8822-8824.
44. Grimme, S.; Ehrlich, S.; Goerigk, L., Effect of the Damping Function in Dispersion Corrected Density Functional Theory. *J. Comput. Chem.* **2011**, 32, 1456-1465.
45. Ghysels, A.; Van Neck, D.; Van Speybroeck, V.; Verstraelen, T.; Waroquier, M., Vibrational Modes in Partially Optimized Molecular Systems. *J. Chem. Phys.* **2007**, 126, 224102.
46. Ghysels, A.; Van Neck, D.; Waroquier, M., Cartesian Formulation of the Mobile Block Hessian Approach to Vibrational Analysis in Partially Optimized Systems. *J. Chem. Phys.* **2007**, 127, 164108.
47. Das Sarma, S.; Adam, S.; Hwang, E. H.; Rossi, E., Electronic Transport in Two-Dimensional Graphene. *Rev. Mod. Phys.* **2011**, 83, 407-470.
48. Froehlicher, G.; Berciaud, S., Raman spectroscopy of Electrochemically Gated Graphene Transistors: Geometrical Capacitance, Electron-Phonon, Electron-Electron, and Electron-Defect Scattering. *Phys. Rev. B* **2015**, 91, 205413.
49. Yan, J.; Zhang, Y.; Kim, P.; Pinczuk, A., Electric Field Effect Tuning of Electron-Phonon Coupling in Graphene. *Phys. Rev. Lett.* **2007**, 98, 166802.
50. Basova, T. V.; Kiselev, V. G.; Schuster, B.-E.; Peisert, H.; Chassé, T., Experimental and Theoretical Investigation of Vibrational Spectra of Copper Phthalocyanine: Polarized Single-Crystal Raman Spectra, Isotope Effect and DFT Calculations. *J. Raman Spectrosc* **2009**, 40, 2080-2087.
51. Li, D.; Peng, Z.; Deng, L.; Shen, Y.; Zhou, Y., Theoretical Studies on Molecular Structure and Vibrational Spectra of Copper Phthalocyanine. *Vib. Spectrosc.* **2005**, 39, 191-199.

Table of Contents (TOC) Image: